GEOPHYSICS, VOL. 72, NO. 1 (JANUARY-FEBRUARY 2007); P. N1–N9, 14 FIGS., 1 TABLE.
10.1190/1.2399458

Field tests of electroseismic hydrocarbon detection

A. H. Thompson[1], Scott Hornbostel[1], Jim Burns[1], Tom Murray[1], Robert Raschke[1], John Wride[1], Paul McCammon[1], John Sumner[1], Greg Haake[1], Mark Bixby[1], Warren Ross[1], Benjamin S. White[2], Minyao Zhou[2], and Pawel Peczak[2]

ABSTRACT

Geophysicists, looking for new exploration tools, have studied the coupling between seismic and electromagnetic waves in the near-surface since the 1930s. Our research explores the possibility that electromagnetic-to-seismic (ES) conversion is useful at greater depths. Field tests of ES conversion over gas sands and carbonate oil reservoirs succeeded in delineating known hydrocarbon accumulations from depths up to 1500 m. This is the first observation of electromagnetic-to-seismic coupling from surface electrodes and geophones. Electrodes at the earth's surface generate electric fields at the target and digital accelerometers detect the returning seismic wave. Conversion at depth is confirmed with hydrophones placed in wells. The gas sands yielded a linear ES response, as expected for electrokinetic energy conversion, and in qualitative agreement with numerical simulations. The carbonate oil reservoirs generate nonlinear conversions; a qualitatively new observation and a new probe of rock properties. The hard-rock results suggest applications in lithologies where seismic hydrocarbon indicators are weak. With greater effort, deeper penetration should be possible.

INTRODUCTION

Electroseismic (ES) surveying is a method for remotely identifying the presence of hydrocarbons using the conversion of electromagnetic energy to seismic energy. A computer-controlled, coded-waveform voltage, applied to electrodes at the earth's surface, causes a current to flow in the subsurface. At certain discontinuities in rock properties, a portion of the electrical current converts to seismic energy. Geophones record the resulting seismic wave at the surface and/or in boreholes (Figure 1).

The spacing of the electrodes is similar to the depth of the target. At a contrast in electrical properties, the vertical component of the electric field is discontinuous. The resulting gradient in field creates a local displacement of the pore-surface dipole layers. The charge displacement creates local, relative flow between the pore and grain spaces or induces a pressure gradient in the rock. This is electrokinetic coupling.

Many mechanisms can create ES coupling. An applied electric field interacts with any internal field in a rock to create ES coupling. The field can also induce second-order coupling through electrostriction. Generally, the literature only discusses electrokinetic coupling; coupling to fluids in dipole layers on pore surfaces.

Hydrocarbon-bearing formations should produce a stronger signal than nearby nonhydrocarbon-bearing formations of the same lithology because hydrocarbons are more resistive than water, and the ions in water and the oil in the pore space are mobile in reservoir rock (Pride, 1994). The largest ES signals will occur where high resistance creates large discontinuities in the vertical component of the electric field and, at the same time, the high-resistance rock contains residual water that has mobile ions. Large signals are not expected from high-resistance rock that contains no mobile water ions or in rocks where the pore space is disconnected so that fluid or ionic transport does not occur over macroscopic distances.

At the present state of technology, the generated signals are weak because of limits in driving large currents into the ground. With better sources and methods, the ES signals can be as large as typical seismic reflections (Thompson and Gist, 1993). The small signals we are currently able to detect must be extracted by signal processing with specially designed source waveforms and via redundant data collection from a noise background several orders of magnitude stronger, as described in Hornbostel and Thompson (2005).

Manuscript received by the Editor March 8, 2006; revised manuscript received September 29, 2006; published online December 13, 2006.
[1]ExxonMobil Upstream Research Co., P.O. Box 2189, Houston, Texas 77252-2189. E-mail: athompson4@houston.rr.com, scott.c.hornbostel@exxonmobil.com, sumnergeo@earthlink.net, warren.s.ross@exxonmobil.com.
[2]ExxonMobil Research and Engineering, Annandale, New Jersey 08801. E-mail: benjamin.s.white@exxonmobil.com, minyao.zhou@exxonmobil.com, pawel.k.peczak@exxonmobil.com.

Electroseismic conversion should be clearly distinguished from the reciprocal process, seismic-to-electromagnetic (SE) conversion. Thompson and Gist (1993 and 1999) discuss the reciprocal processes and the fact that, although the linear responses are predictably reciprocal processes, one process may be more practical to implement than the other, and they may give different information about the reservoir properties. We have found that ES has certain field-application advantages.

Three properties favor large amplitude conversions between seismic and electromagnetic energies: (1) contrast in acoustic impedance, (2) permeable pore space, and (3) high-resistivity pore fluids. Of these three, the contrast in acoustic impedance may be the weakest determinant of amplitude for SE conversion. Seismic reflection coefficients are small, often less than 1%. Most of the incident seismic energy propagates through the target interface unperturbed. Small seismic reflection coefficients favor using the inverse process, electroseismic conversion.

Contrasts in viscosity, porosity, and elastic properties are not expected to yield large ES signals. Contrasts in permeability may be important because extremely small permeabilities are not ES active. The theory of ES conversion (Pride, 1994) suggests that permeability is a second-order contributor to the conversion amplitude. However, the permeability and electrical properties are related to each other in rock so that the permeability and conductivity sensitivities are not generally separable. Other properties that are indirectly related to electrical properties may be important to ES conversion. For example, wettability changes may create large contrasts in electrokinetics. Boundaries between different lithologies will induce gradients in the chemical potential that create internal electric fields. Compressible fluids and gradients in diagenetic alteration will also be important.

Despite this host of possible influences on ES coupling, the largest single influence on amplitude of conversion in a single rock type will be the conductivity of the pore fluids, and hence the hydrocarbon saturation. Numerical models of the full conversion process from electromagnetic to seismic waves indicate that 20% oil saturation may increase the ES amplitude by a factor of ten.

The ES method has been under active investigation by ExxonMobil and a few other researchers for several years. The reader is referred to Thompson and Gist (1993 and 1999), Pride (1994), Hornbostel and Thompson (2002), Hornbostel et al. (2003), Deckman et al. (2005), Thompson (2005), and White (2005) for background on the underlying principles of the method. In the present paper, we summarize the results of three field tests of the method. Field tests 1 and 2 show application of the method to shallow gas sands, at depths up to 1000 m. Field test 3 shows application to a deeper carbonate oil reservoir.

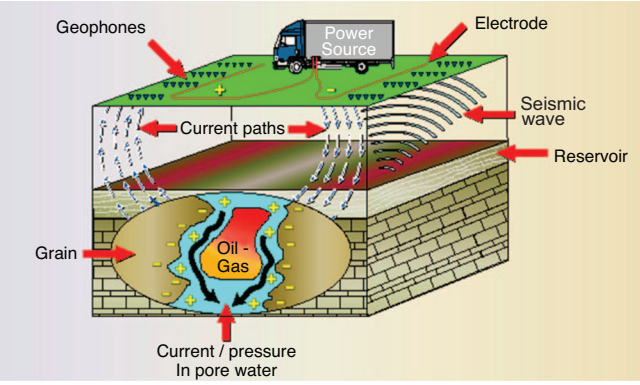

Figure 1. Description of the ES method. A current injected into the subsurface creates local field gradients at discontinuities in electrical properties. Applied fields couple to internal rock fields, including fields in the dipolar boundaries on pore surfaces. This electrokinetic coupling displaces the dipolar fluid layers causing relative movement or pressure generation in the grain space.

FIELD TEST RESULTS

Field example 1: Webster, Texas

The Webster field is located along the Texas Gulf Coast, 20 mi southeast of the city of Houston. Though the primary production at Webster is from the Frio formation, gas was produced from five shallow zones. These sands occur in the Pleistocene age Beaumont and Lissie formations deposited in fluvial and deltaic systems. They are unconsolidated with porosities of up to 34%.

The ES experiments were conducted to detect possible responses from these shallow gas targets. The ES 3D surface survey covers an area of 0.2 km^2. A typical field test layout is shown in Figure 2. The power source in the center of the figure is connected to a power line

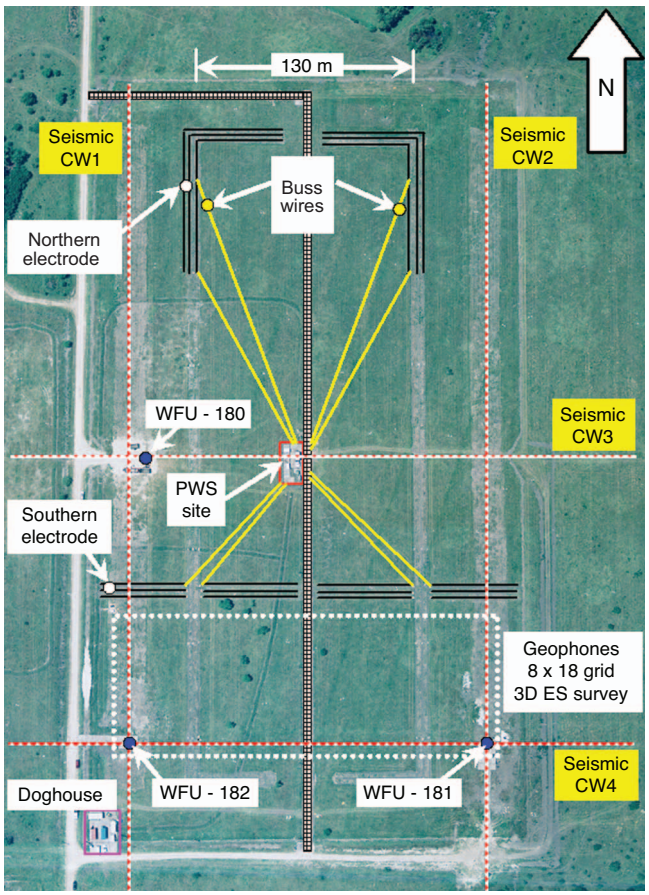

Figure 2. Typical field layout for Webster field test. A power waveform synthesizer (PWS) is located in the center of the layout and is connected to the north and south electrodes by bus wires (yellow). The north electrode (two inverted L-shaped electrodes separated by a space) and the south electrode (straight east-west-running electrode) are at opposite voltages. Four 2D seismic lines (two north-south and two east-west) are shown in red. A 3D ES survey was collected with eight east-west geophone lines of 18 geophones each placed south of the south electrode.

and has outputs connected to buried electrode wires via bus wires. The angular electrodes at the north are at one polarity while the east-west segments to the south are at the opposite polarity. In addition to the red 2D seismic lines depicted in the figure, a 3D ES survey was conducted with geophones south of the south electrode. We also collected a 3D seismic survey.

Figure 3 compares a portion of the ES data to the corresponding seismic data and to a stratigraphic interpretation based on well data in the field (the WFU wells in Figure 3). The ES response begins below the shale response and illuminates the gas sand interval. This figure shows ES responses associated with the 320-sand and the 350-sand at WFU-182. (The numbers in the sand formation names refer to the depth of the sand in feet.) The figure also shows an ES response associated with the top of the 450-sand on this line. ES data acquired using downhole receivers in the WFU-182 well also show a response from the gas sands.

Figure 4 shows a 3D perspective view of large amplitude ES responses inserted into the 3D seismic survey. The top two blue ES responses correspond to the 320-/350-sand and the 450-sand, respectively. As in Figure 3, the labeled high-amplitude seismic horizon corresponds to a laterally extensive high-impedance shale layer just above the gas sands. There is no strong seismic response at the actual depths of the gas sands. The top two ES responses closely correlate with the known gas sands. There are three deeper ES responses that, at the time of the survey, were not known to be present at this location because no well had penetrated them.

After the ES survey was completed, a deeper well (indicated by the yellow line in Figure 4), the WFU-183 well, was drilled and logged. This well penetrated the deeper sands. Figure 5 shows log curves superimposed on the ES data. The WFU-183 log confirms the presence of resistive sand intervals at the depths of the deeper ES responses. Seismic and well data indicate that the 320-sand extends across the entire line. A channel has eroded into the 350-sand to the east of the WFU-182 and subsequently filled with shale. This well confirmed the interpretation that the 350-sand would not be present at this location. The well also encountered low-gas saturations in a 31-m sand at 140 m, a 12-m sand at 250 m, and a 6-m sand at 285 m. The latter two gas sands correlate with the previously identified deeper ES events at 320 ms and 370 ms, respectively.

We now consider the 1D and 3D modeling of the ES responses. The model used for comparison of simulated 1D ES responses with the field data is based on well WFU-182. The model is horizontally layered and includes the upper two gas sands. Table 1 shows details of the layered model. The model response to this layered structure is computed using a 90° phase-rotated 40-Hz Ricker wavelet, which approximately matches the amplitude and phase spectrum of the processed data. ES model responses are computed at 144 surface locations corresponding to those in the field data. The field and model data are averaged over all traces for comparison.

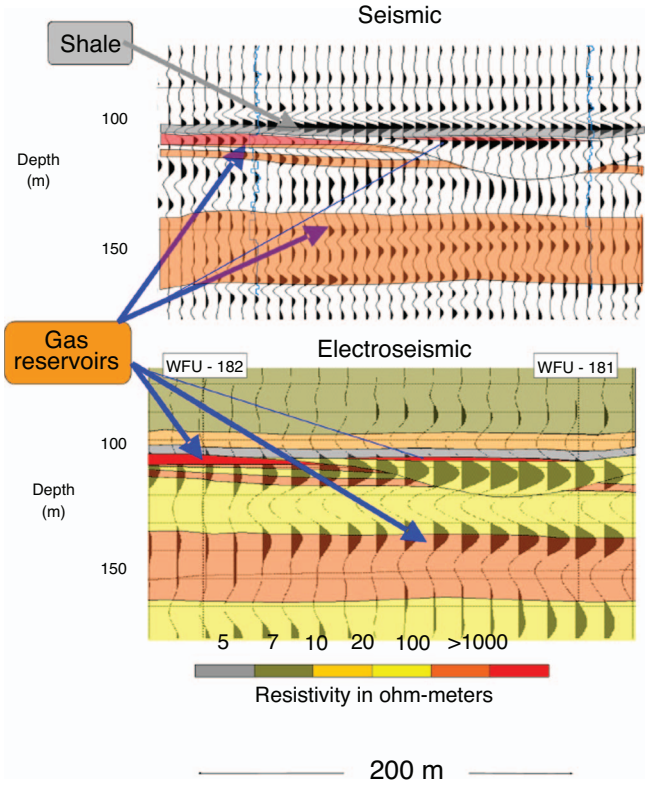

Figure 3. Webster field. Seismic, ES, and stratigraphic interpretation. The upper seismic display from the 3D seismic survey shows large amplitude response to the shale above the gas sands. The lower ES display shows large amplitude response to the gas sands.

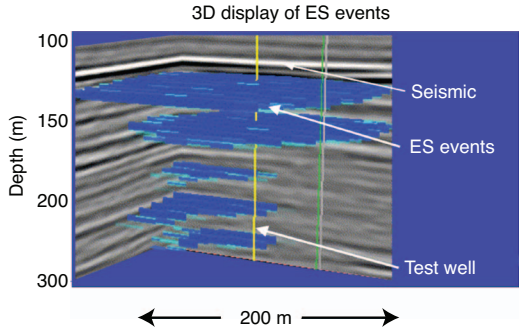

Figure 4. Webster field. Perspective view of large amplitude ES responses inserted into 3D seismic survey.

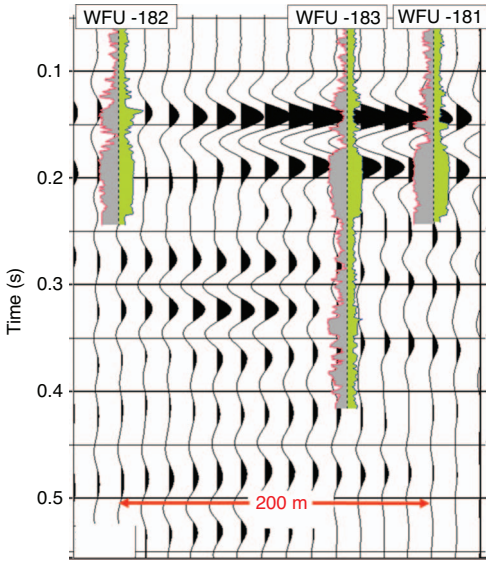

Figure 5. Webster field. Deeper ES events and well logs. The middle well log is from the WFU-183 well, drilled after the survey was shot to confirm the presence of deeper gas sands correlative with the ES events.

Figure 6 shows the average response as computed by modeling with the average response of the data for a depth corresponding to the top two sands. The two gas sands are not individually resolved at this frequency but are characterized by a large oscillation where the base of the upper sand and the top of the lower sand merge to produce a single trough at 130 m. Because the lower gas sand is much thicker (31 m versus 15 m for the upper sand), its base is individually resolved as a trough at about 175 m. Following the gas sand responses are oscillations representing acoustic reverberations (internal multiples) set off by the primary ES responses and their repeated interactions with the layering. The model response must be scaled by a factor of five to match the data amplitude. With that scaling, the match is reasonably good in timing and general character. The only real character difference between the two is that the base of the deeper gas sand is more sharply defined in the model response than it is in the field-data response.

At present, we do not have a definitive explanation for the factor of five amplitude mismatch. We have observed a similar underprediction of field amplitudes in several cases. We hypothesize that lack of detail in the models, or lack of information about the right parameters (e.g., permeabilities, conductivities, gas saturations), explains the difference. Layered models of ES conversion show that a layer of gas only 10 cm thick doubles the modeled response. The influence of thin compressible layers can also be large. A 5-cm-thick layer of very low conductivity increases the response tenfold.

Whichever of these or potentially several other effects are present with thin layers, it is not simply a matter of using the full resolution of the logging-tool data. We have remodeled the above responses with all beds in the original logs, which results in essentially identical amplitudes. Whatever might explain the particular amplitudes at the Webster site is below the resolution of the logging tool, related to inaccuracies in the choice of model parameters, or related to the 1D model limitations.

Some aspects of the model and field results require consideration of 3D effects. For example, if the cross-sectional model as shown in Figure 3 is accurate, and there are no unaccounted for gas pockets toward the right of the section, one would expect the ES event to weaken over the shale-filled channel. As shown in the figure, however, the event from the 350-sand in the WFU-182 continues and strengthens across the channel to the WFU-181 where the 350-sand does not exist. There are several explanations for this result:

1) Surface geophones closer to the center of the electrode array record a stronger response than geophones near the edges.
2) Higher resistivities at the surface near WFU-182 and over the 350-sand reduce the current flux and, hence, the ES response.
3) Gas in the 350-sand actually guides the current to the perimeter of the gas sand, thus reducing the response over the gas sand.

We eliminated electrode response functions and near-surface resistivity variations as causes of the strengthening of the ES event, though they do affect amplitudes. The electrode response (the electric-field illumination pattern) is strongest at the electrode center and weakens uniformly at both ends and at offsets perpendicular to the electrode. There is no preferential east-west dependence. Even after normalization for the electrode arrays, the ES response remains weak for the gas-charged 350-sand at the WFU-182.

Higher resistivities at the surface may also affect the ES amplitudes. A shallow resistivity survey was conducted using shallow induction tools (EM-31, EM-38), and it was found that the average resistivity over the survey area is 8–10 ohm-m. There is an area of high resistivity (12–15 ohm-m) in the southwest portion of the ES survey that coincides with the area around the WFU-182. The higher resistivity in this area limited the current passing into the ground from the electrode and resulted in a weaker ES response. Several different solutions were attempted to mitigate the problem, but the effect of the shallow, resistive area persisted in the data. Nonetheless, the normalization by both this resistivity ratio and the electrode response function did not eliminate the ES amplitude variation observed in the data.

Three dimensional models of the ES response indicate that the higher resistivities associated with the gas in the 350-sand at the WFU-182 may displace the current lines to the edges of the gas sand. The 3D modeling was performed using the method discussed in White (2005). The importance of current steering is situation dependent. The reservoir depth, size, thickness, and resistivity control the degree to which this phenomenon is important. In the Webster example, 3D modeling is possibly less accurate than desired because the depth, electrode separation, electrode size, and reservoir structure all have similar dimensions.

In summary, this first survey detected shallow gas sands and identified several gas sands deeper in the section that were not identified prior to the survey but were subsequently confirmed by drilling a postsurvey well. One-dimensional ES model responses match the character of the field-data responses but are low by a factor of five in overall amplitude. For this combination of reservoir depth, resistivity, thickness, shape, and lateral extent, and within the resolution of a 3D model, currents are steered towards the edge of the reservoir, illuminating most brightly the parts where the reservoir is thinnest.

This is the first successful demonstration that ES can distinguish between aquifers and gas

Table 1. The layered model used to calculate the ES response at Webster.

Depth (m)	Conductivity (S/m)	V_p (m/s)	Perm (m^2)	L ($m^2/V - s$)	Porosity
0	0.04	1524	1e − 16	1e − 16	0.39
30	0.1	1646	1e − 18	1e − 16	0.385831
107	0.02	976	1e − 13	1e − 09	0.375131
122	0.1	1646	1e − 18	1e − 16	0.373046
137	0.02	976	1e − 13	1e − 09	0.370962
168	0.13	1829	1e − 18	1e − 16	0.366654
244	0.13	2012	1e − 16	1e − 16	0.356092
396	0.25	2134	1e − 16	1e − 16	0.334969
549	0.5	2287	1e − 16	1e − 16	0.313708
610	0.67	2378	1e − 16	1e − 16	0.305231
1311	1	2591	1e − 18	1e − 16	0.207815
1707	0.05	2439	1e − 13	1e − 09	0.152785
1799	1	2744	1e − 18	1e − 16	0.14
4000	0.1	2744	1e − 16	1e − 16	0.14

sands. There are no reports in the literature prior to this work that document electromagnetic-to-seismic conversion and none that use surface-mounted equipment to detect hydrocarbons at these depths.

Field example 2: Turin, Alberta, Canada

The Turin field is located in Southern Alberta. The Lower Cretaceous Glauconitic Sand produces oil in point-bar sands deposited as valley fill in an estuarine environment. The reservoir is at 1000-m drill depth and has porosities as high as 28%, permeability up to 4 darcies, and maximum net sand thickness of 35 m. Both surface and downhole data in the vicinity of two wells, the Turin 12-14 and the Turin 8-15, were acquired to compare ES responses over a very thin oil leg (essentially wet reservoir) and a thin oil leg overlain by a thick gas cap, respectively. Figure 7 shows the stratigraphy and fluid content in each well.

Figure 8 shows the ES responses at the two locations. The measured trace on the right side of both Figure 8a and b is a stacked trace that is the sum of thousands of acquired traces, processed to sum all repetitions and all geophone stations together (after noise editing) to produce one final trace representing the ES response of the subsurface at each location. Four different types of source waveforms were used to generate sweeps, two at approximately 8 Hz, one at 18 Hz, and one at 25 Hz. The model trace in the figure was computed via the layered-modeling method using the waveform corresponding to one of the lowest frequency sweeps at 8 Hz. Three-dimensional electric-field modeling was performed to confirm relatively uniform illumination of the sands, thus eliminating the need for full 3D modeling of the ES response. The stacked and model traces are converted to depth for comparison to well data using sonic log velocities.

The total equivalent field effort is different for the two locations. After trace editing, the effective field effort at Turin 8-15 was greater by a factor of six. Each trace has a noise bound posted (red lines) that incorporates the expected noise level for each set of experiments, derived from the standard deviation of the amplitude of all the prestack traces at each time sample. For the Turin 8-15 surface data, 143,000 traces are stacked together to obtain the final trace. A time taper was applied to the traces to ensure that below 300 ms only the 54,482 lowest-frequency traces contribute to the sum. Prior to stacking, these traces are essentially noise. Hence, at each time sample, there are 143,000 samples from the noise distribution. The distribution was plotted and confirmed to be approximately Gaussian. At each time sample, the standard deviation of the samples in the stack (accounting for the time taper) was computed and converted to a 95% confidence interval using the Gaussian distribution, plotted as the red line. An equivalent calculation was done for the 50,000 traces at the Turin 12-14 location.

In both cases, strong shallow ES events are visible above the confidence bound. These events originate at the water table or some shallow layer that is illuminated with a very strong local electric field (before decay with depth). The differences between the two traces are most apparent at the reservoir level. The Turin 12-14 trace has oscillations at all times, but they are contained within the noise bounds, which means no signal is statistically significant at any depth below the shallow arrivals. The Turin 8-15 trace also has oscillations throughout time. For most of the trace, those oscillations are also contained within the noise bounds. At the reservoir level, however, a distinct event is present. This event has a 95% probability of being a real arrival rather than an oscillation related to residual random noise.

For the Turin data, the mismatch in predicted and measured amplitudes is much larger than for Webster. The model amplitudes underpredict the observed data by several orders of magnitude. Unfortunately, the level of field effort used in acquiring these surface data was not high enough to definitively resolve issues about the absolute amplitude of the signals.

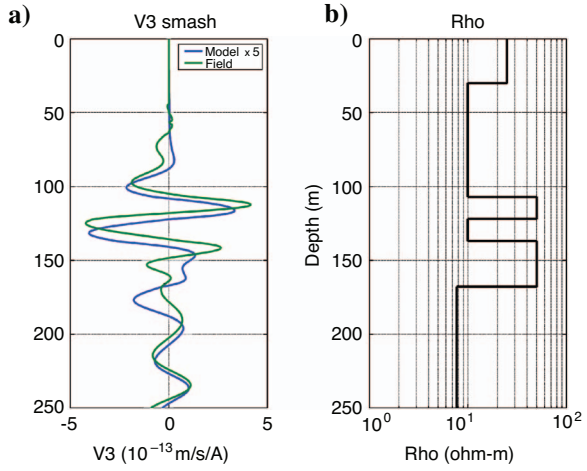

Figure 6. (a) ES field versus (b) model data for a smash of all traces in the survey. Model data is scaled up by a factor of five.

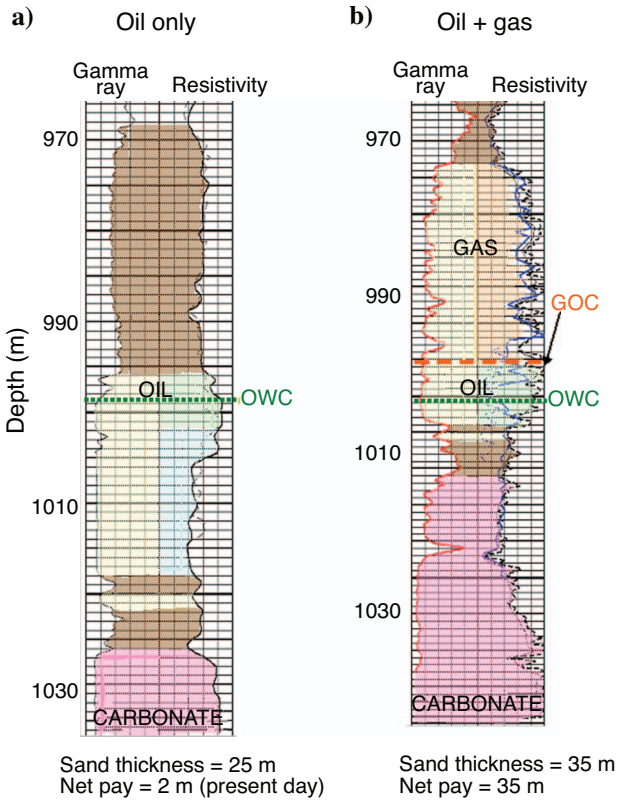

Figure 7. Stratigraphy at the (a) Turin 12-14 and (b) Turin 8-15 wells. The Turin 12-14 well has a thin oil leg. The Turin 8-15 well has a thin oil leg overlain by a thick gas cap. In both logs, the oil-water contact (OWC) is indicated shallower than the logs show because the present-day OWC has moved upward relative to where it was when the wells were logged.

The primary purpose of the Turin experiments was to acquire ES data in several wells. Downhole ES responses were observed in earlier field tests where they were of very good quality, required less field effort to acquire than surface ES data, and correlated with hydrocarbons. Downhole responses are recorded with hydrophones, which respond to the tube waves generated at ES conversion points in the subsurface.

Figure 9 shows an example of these responses at the Turin 12-14 well. The inverted V-shaped pattern to the tube waves, which emanate from discrete depth levels and travel up and down the borehole, are very clear in these data. The S/N is very high due to the quiet downhole environment and the large amplitude of tube waves. In the unscaled record, the largest response comes from the bottom of surface casing. There is also a response from a zone labeled the "heterogeneous" zone, which is a zone of rapid oscillation in a through-casing resistivity log acquired near 500 m depth. This heterogeneous zone has the largest response in the record after scaling by the expected decay of the electric field with depth. There are other responses at depth in the scaled version, and there may be a small reservoir-related signal as well, indicated by ®.

To test whether the heterogeneous zone response in the record at 500 m was caused by hydrocarbons, we perforated and stimulated several intervals that had high resistivity in the through-casing log. No hydrocarbons were found. After reinspecting the cement-bond logs, our posttesting interpretation is that a slight degradation in the cement bond behind casing generated the response from the zone, and likely generated the oscillations in the through-casing log as well.

Figure 10 shows downhole data for the Turin 8-15 well. This well had a variable water level, and at the time of acquisition, the average water level was at a depth of about 350 m. An ES response is present from this depth. On the scaled record, the largest ES response is from a depth of 670 m and is near the top of the lower Cretaceous. There are also deeper responses. A signal from the reservoir level is visible, though its strength is not observably larger than the reservoir signal in the Turin 12-14 well.

In both cases of downhole data, although there may be weak hydrocarbon-related responses, the most prominent responses are from discontinuities in subsurface or near-borehole properties. Such responses may be useful as indications of cement-bond quality, borehole state, or properties of the subsurface in the vicinity of the borehole.

In summary, this second shallow gas-sand survey was most likely successful at discriminating the presence or absence of hydrocarbons at a depth of 1000 m. This is more than double the depth achieved for the deepest observed gas sand in the Webster field test. Field effort was much lower than that at Webster but sufficient to show indications of an ES response to a thick, highly resistive gas cap. Evidence that signal is present comes from comparing the final stacked trace as well as subsets of the data to noise bounds, all of which show that a cycle at the right time for the reservoir is present above the noise. The residual noise shows all indications of being uncanceled random noise and may thus be overcome by a higher field effort.

Downhole data, acquired during the Alberta experiments, clearly illustrate evidence for ES conversions because of the characteristic inverted-V signals indicative of up- and downgoing tube waves emanating from several depth levels starting at zero time. No mechanical disturbance or elastic wave could reach those depth levels in this short a time interval. The ES conversions may or may not be indicative of hydrocarbons. Frequently, they are conversions from borehole-related structures, stratigraphy, or subsurface conditions restricted to the vicinity of the borehole.

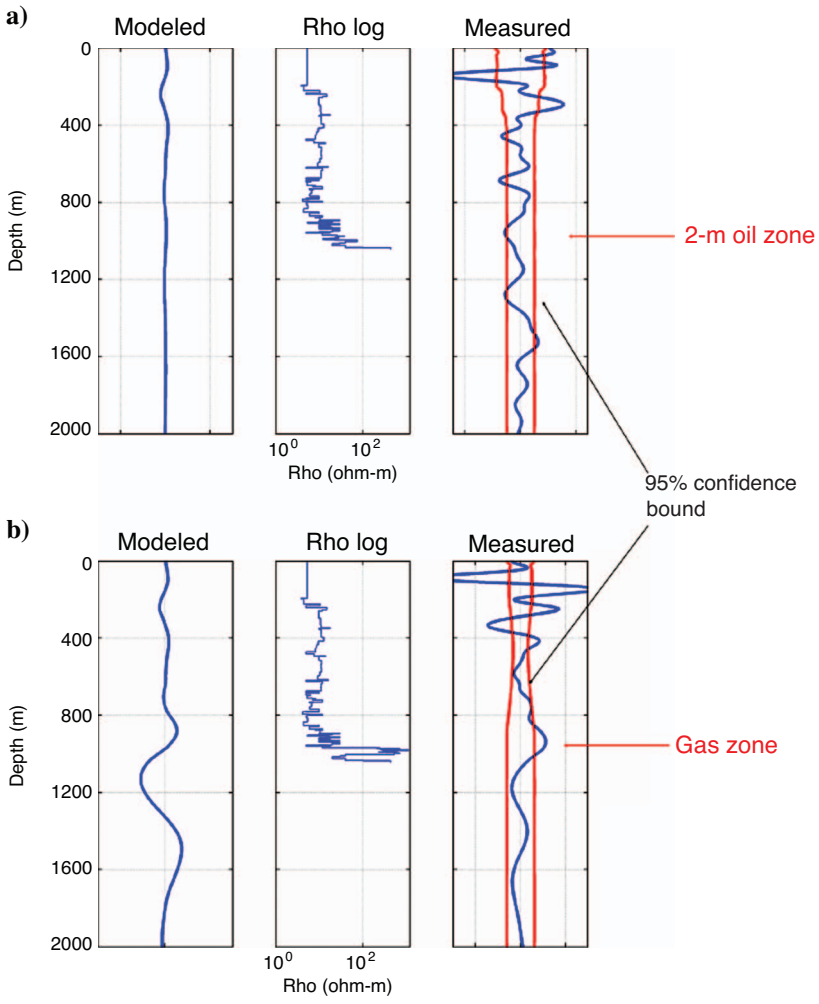

Figure 8. ES response for (a) thin oil zone versus (b) thick gas zone.

Field example 3: Bronte, Texas

The Bronte field is located on the Eastern Shelf of the Midland Basin in Coke County, Texas. Bronte represents a significant departure from the previously discussed field tests, differing from Webster and Alberta in depth, rock type, and hydrocarbon fluid. There are five stacked reservoir formations shown in Figure 11. The Palo Pinto, Capps, Goen, and Cambrian formations produce oil, while the Gardner produces gas. Reservoir

depths range from 1310 to 1615 m. Porosities range from 6% to 12%. Permeability ranges from 7 to 200 millidarcies. Net pay thickness averages 11 m.

The pay interval has average resistivity of 250 ohm-m in the Palo Pinto and Cambrian formations, but only 25 ohm-m for the Capps, Goen, and Gardner formations. Low porosity and thin net pay found in all the producing intervals and the low resistivity for three of the producing intervals suggest a weak ES linear response from these pay zones, even with the benefit of good electric-field illumination resulting from a resistive overburden. This weak response is confirmed by comparing acquired ES data to logs, shown in Figure 11. The response at the Palo Pinto is not much stronger than background responses or the response in the middle of the shale section above the reservoir. Modeling of the expected ES amplitude also shows very weak response, but because such modeling regularly underpredicts observed ES field amplitudes, this weak model response adds no additional confirmation of the above observations.

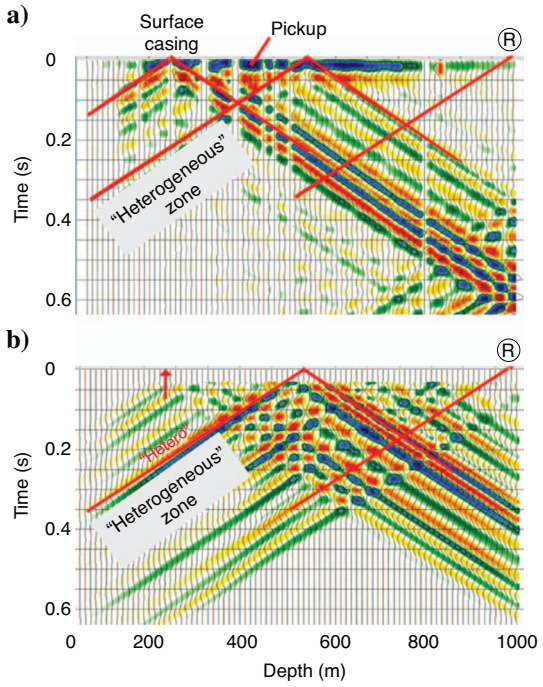

Figure 9. Downhole data in the Turin 12-14 well. (a) Unscaled data after correlation, (b) data scaled by time squared (T^2).

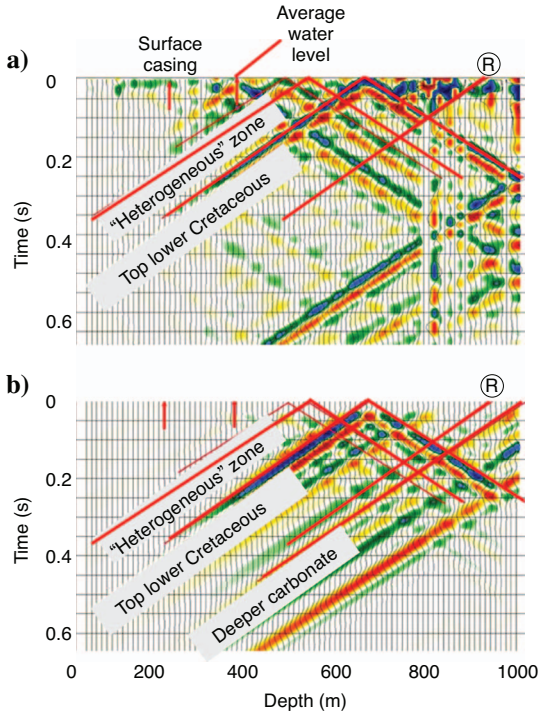

Figure 10. Downhole data in the Turin 8-15 well. (a) Unscaled data after correlation, (b) data scaled by time squared (T^2).

Thus far, we have been discussing what we call the linear ES response, namely the response consistent with the linear theory of electrokinetics as described by Pride (1994). Other conversion mechanisms (Hornbostel et al., 2003) provide the theoretical basis for nonlinear ES responses, which we pursued in lab and field studies. In well measurements, the second harmonic had better S/N and appeared to have better hydrocarbon discrimination than the standard linear data. As a result, we developed special source waveforms designed to highlight nonlinearity (Hornbostel and Thompson, 2005), and we collected a 3D ES survey using them.

The nonlinear data set had better S/N and was more coherent with the reservoir than was the original linear data set. Figure 12 shows line 11 from the nonlinear 3D ES survey. This line shows weaker responses from two of the other reservoirs and shallow, but incoherent, ES responses we attribute to noise spikes.

Figure 13 shows an aerial view of the nonlinear ES response at the Palo Pinto reservoir. The Palo Pinto amplitudes are confined to the west (upthrown) side of the Fort Chadbourne Fault, which is known to be the boundary of production. This is a confirmation of the presence of coherent nonlinear ES signal only where production occurs. The variability of amplitudes within the reservoir is considered significant, but the cause is unknown, possibly a result of enhanced porosity, facies variations in the carbonates, or bypassed oil. Two additional time slices are compared to the Palo Pinto time slice in Figure

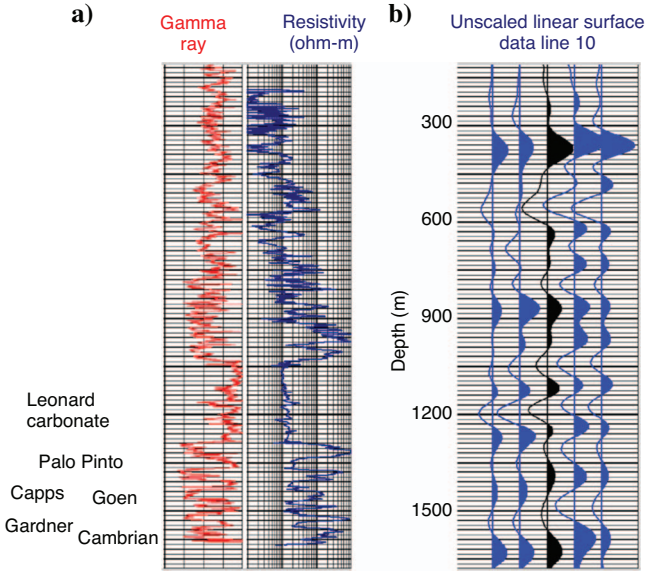

Figure 11. Bronte field. (a) Well logs and (b) linear ES data. Surface data are corrected to depth using well check shots. The black is the trace at the location of the well.

14. The time slice on the Cambrian reservoir is less coherent than the Palo Pinto time slice, but amplitudes are still mostly confined to the western side of the fault. The nonreservoir basement reflector has low ES amplitude and appears similar in amplitude on both sides of the fault.

This third ES survey stretched the limits of the linear ES technology from the earlier surveys, attempting to discriminate hydrocarbons at deeper depths, in carbonates, and in oil-filled reservoirs. At our present level of effort, the linear data collected at Bronte are not usable in creating a 3D image. The nonlinear response did provide a 3D image that conforms to production at one of the reservoir levels. In particular, the nonlinear response on the Palo Pinto reservoir is confined to a portion of the survey area with hydrocarbons, whereas nonlinear responses on nonreservoir horizons exhibit much more patchy amplitudes.

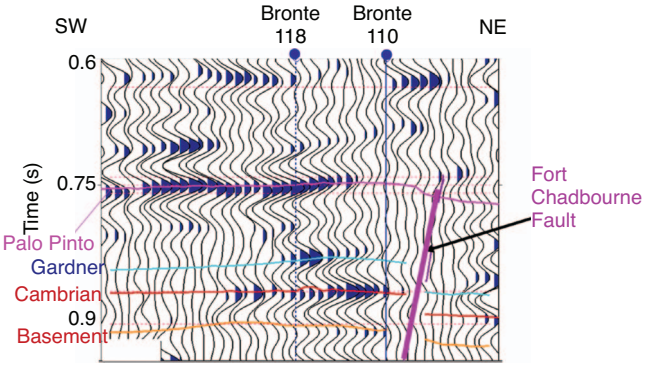

Figure 12. Bronte field. Nonlinear ES response for line 11. Location of line 11 is shown on the map in Figure 13.

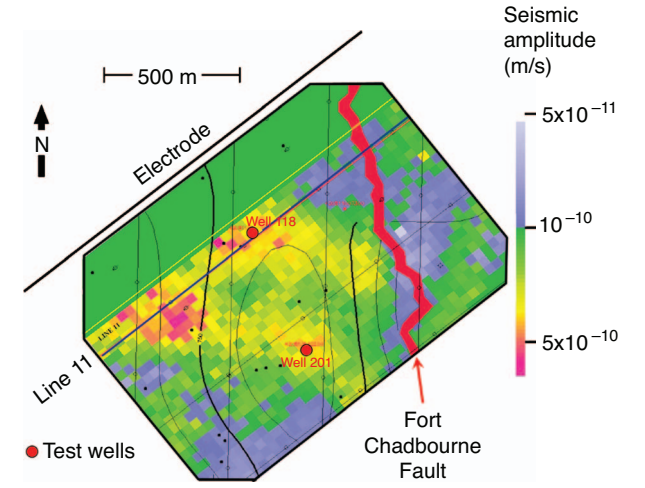

Figure 13. Bronte field. Aerial view of the nonlinear ES response on the Palo Pinto reservoir.

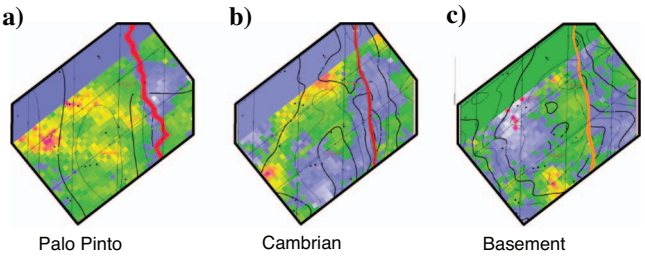

Figure 14. Bronte field. Nonlinear ES response on three time slices: (a) the Palo Pinto reservoir, (b) the Cambrian reservoir, and (c) a basement reflection (nonreservoir).

CONCLUSIONS

Two field tests of the ES method have shown that the conversion of electromagnetic energy to seismic energy at gas sands 500 m deep, and possibly as deep as 1000 m, can be detected with geophones placed on the surface of the earth. The detected seismic energy is at the same frequency as the source electrical power. Models based on an electrokinetic conversion mechanism and field data agree qualitatively, if not in absolute amplitude.

A third field test at the Bronte Field detected second-order ES conversions from reservoirs greater than 1500 m deep. The ES signal was used to map the reservoir. Second-order conversions double the frequency of the electromagnetic source leading to enhanced spatial resolution. This is the first time second-order conversions have been detected in field data. The coherence of the amplitudes at the reservoir interval and the lack of coherence of the amplitudes elsewhere support the interpretation of the second order conversions and stimulate interest in further investigations.

The nonlinear response is a new phenomenon and is not fully understood. It is not obvious that the electrokinetic conversion process can account for second-order effects. Further work is required to develop theoretical explanations of second-order conversion and to determine what mechanism generated the second-order conversions at Bronte.

Detecting second-order responses at Bronte was made possible, in part, because processing for the second-order signal enhances the rejection of source noise. With the equipment and methods employed at Bronte, we were unable to detect the reservoir with the linear ES method. Experience gained in this field work leads us to predict that numerous advances in equipment and methods are possible. Further work is needed to determine if first-order conversions are detectable from depths greater than 1000 m in lithologies similar to Bronte.

Well tests at Turin showed ES conversions from depth. Most of the detected responses are indications of borehole properties such as cement-bond quality, casing junctions, etc. Some may be indications of stratigraphy or near-borehole conditions. In other well tests at Bronte and Webster, we clearly observed the ES conversions in the formation. We conclude that ES well tests may be useful in diagnosing well properties, including cement integrity and near-well ES conversions.

More generally, the entire field of electroseismic technology, both linear and nonlinear, warrants further investigation based on its potential and the qualitatively new observations presented herein.

ACKNOWLEDGMENTS

We acknowledge the cooperation of ExxonMobil Canada for assisting during the field tests and for approval to publish the results. We thank our many colleagues at ExxonMobil Upstream Research and ExxonMobil Corporate Strategic Research who contributed to this project over many years, especially Eric Herbolzheimer, Harry

Deckman, Mark Ephron, John Dickinson, Grant Gist, and Max Deffenbaugh.

REFERENCES

Deckman, H. W., E. Herbolzheimer, and A. Kushnick, 2005, Determination of electrokinetic coupling coefficients: 75th Annual International Meeting, SEG, Expanded Abstracts, 561–564.

Hornbostel, S. C., and A. H. Thompson, 2002, Source waveforms for electroseismic exploration: U. S. Patent 6,477,113 B2.

——–, 2005, Waveform design for electroseismic exploration: 75th Annual International Meeting, SEG, Expanded Abstracts, 557–560.

Hornbostel, S. C., A. H. Thompson, T. C. Halsey, R. A. Raschke, and C. A. Davis, 2003, Nonlinear electroseismic exploration: U. S. Patent 6,664,788 B.

Pride, S., 1994, Governing equations for the coupled electromagnetics and acoustics of porous media: Physical Review B, **50**, 15678–15696.

Thompson, A. H., 2005, Electromagnetic-to-seismic conversion: Successful developments suggest viable applications in exploration and production: 75th Annual International Meeting., SEG, Expanded Abstracts, 554–556.

Thompson, A. H., and G. A. Gist, 1993, Geophysical applications of electrokinetic conversion: The Leading Edge, **12**, 1169–1173.

——–, 1999, Geophysical prospecting: U. S. Patent 5,877,995.

White, B. S., 2005, Asymptotic theory of electroseismic prospecting: IMA Journal of Applied Mathematics, **65**, 1443–1462.